ADVANCES IN ATMOSPHERIC SCIENCES, VOL. 35, FEBRUARY 2018, 234–247

• **Original Paper** •

Aerosol Microphysical and Radiative Effects on Continental Cloud Ensembles

Yuan WANG*[1,5], Jonathan M. VOGEL[2,6], Yun LIN[2], Bowen PAN[2], Jiaxi HU[2], Yangang LIU[3], Xiquan DONG[4], Jonathan H. JIANG[5], Yuk L. YUNG[1,5], and Renyi ZHANG[2]

[1]*Division of Geological and Planetary Sciences, California Institute of Technology, Pasadena, CA* 91106*, USA*
[2]*Department of Atmospheric Sciences, Texas A&M University, College Station, TX* 77840*, USA*
[3]*Environmental & Climate Sciences Department, Brookhaven National Laboratory, Upton, NY* 11973*, USA*
[4]*Department of Hydrology and Atmospheric Sciences, University of Arizona, Tucson, AZ* 85721*, USA*
[5]*Jet Propulsion Laboratory, California Institute of Technology, Pasadena, CA* 91109*, USA*
[6]*Department of Atmospheric and Oceanic Sciences, McGill University, Montreal, Quebec QC H*3*A* 0*G*4*, Canada*

(Received 12 April 2017; revised 7 August 2017; accepted 23 August 2017)

ABSTRACT

Aerosol–cloud–radiation interactions represent one of the largest uncertainties in the current climate assessment. Much of the complexity arises from the non-monotonic responses of clouds, precipitation and radiative fluxes to aerosol perturbations under various meteorological conditions. In this study, an aerosol-aware WRF model is used to investigate the microphysical and radiative effects of aerosols in three weather systems during the March 2000 Cloud Intensive Observational Period campaign at the US Southern Great Plains. Three simulated cloud ensembles include a low-pressure deep convective cloud system, a collection of less-precipitating stratus and shallow cumulus, and a cold frontal passage. The WRF simulations are evaluated by several ground-based measurements. The microphysical properties of cloud hydrometeors, such as their mass and number concentrations, generally show monotonic trends as a function of cloud condensation nuclei concentrations. Aerosol radiative effects do not influence the trends of cloud microphysics, except for the stratus and shallow cumulus cases where aerosol semi-direct effects are identified. The precipitation changes by aerosols vary with the cloud types and their evolving stages, with a prominent aerosol invigoration effect and associated enhanced precipitation from the convective sources. The simulated aerosol direct effect suppresses precipitation in all three cases but does not overturn the aerosol indirect effect. Cloud fraction exhibits much smaller sensitivity (typically less than 2%) to aerosol perturbations, and the responses vary with aerosol concentrations and cloud regimes. The surface shortwave radiation shows a monotonic decrease by increasing aerosols, while the magnitude of the decrease depends on the cloud type.

Key words: aerosol-cloud-radiation interactions, cloud-resolving model, cloud microphysics and macrophysics, precipitation

Citation: Wang, Y., and Coauthors, 2018: Aerosol microphysical and radiative effects on continental cloud ensembles. *Adv. Atmos. Sci.*, **35**(2), 234–247, https://doi.org/10.1007/s00376-017-7091-5.

1. Introduction

The influence of atmospheric aerosols on the energy budget and hydrological cycle remains one of the least understood aspects in the earth system. Aerosols, from both natural and anthropogenic sources (Zhang et al., 2004; Levy et al., 2013), directly scatter and absorb incoming solar radiation, which alters the vertical atmospheric temperature structure, surface and top of the atmosphere (TOA) radiation fluxes, and cloud fraction (Ackerman et al., 2000; Fan et al., 2008). The large uncertainty in the aerosol direct effect is related to the particle size, chemical composition, and mixing state (Khalizov et al., 2009; Zhang et al., 2015; Peng et al., 2016). Depending on those complicated factors, aerosols impose a net positive or negative forcing over different regions. Presently, the aerosol direct forcing is estimated at a global mean of -0.27 W m^{-2} (IPCC, 2007). In addition to the direct radiative effect, absorbing aerosols have a positive feedback that reduces cloud coverage; namely, the semi-direct effect (Hansen et al., 1997; Johnson et al., 2004). The presence of absorbing aerosols in a given vertical layer decreases the atmospheric instability and reduces ambient relative humidity through diabatic heating of the air. This, in turn, enhances cloud evaporation and inhibits convection and vertical mixing, thereby hindering cloud formation, reducing radiative cooling at the TOA, and eventually leading to a positive radiative forcing (Ackerman et al., 2000; Wang et al., 2013a).

By acting as cloud condensation nuclei (CCN) or ice nuclei (IN), aerosols affect the micro- and macrophysical prop-

* Corresponding author: Yuan WANG
Email: yuan.wang@caltech.edu

erties of different types of clouds, impacting their radiation, dynamics, precipitation, and lifetime. The first indirect effect is primarily related to the impact of aerosols on the cloud droplet size and number (Twomey, 1977; Albrecht, 1989; Zhang et al., 2007; Yuan et al., 2008). It has been widely accepted that through the first indirect effect, higher concentrations of aerosols lead to higher concentrations of CCN and cloud droplets. Changing the number and size distribution of cloud droplets due to aerosols consequently alters the vertical depth and lifetime of clouds as well as precipitation processes, which is commonly known as the second indirect effect (Albrecht, 1989; Pincus and Baker, 1994; Fan et al., 2007a, 2007b). By changing the size distribution, the growth of cloud droplets by collision/coalescence becomes suppressed, which reduces drizzle and prevents the loss of cloud water content, leading to an increased cloud lifetime (Albrecht, 1989; Rosenfeld, 1999). For certain types of cloud like trade wind cumulus, the reduced precipitation results in deeper cloud layers but smaller cover due to the stronger evaporation (Seifert et al., 2015). Hence, such an effect buffers the aerosol lifetime effect (Stevens and Feingold, 2009). In mixed-phase clouds, polluted conditions suppress warm-cloud processes but enhance convective development through the aerosol invigoration effect (Rosenfeld et al., 2008; Koren et al., 2010; Tao et al., 2012; Wang et al., 2011; Fan et al., 2012), leading to enhanced cloud electrification and lightning activity (Williams et al., 1991; Nesbitt et al., 2000; Orville et al., 2001). A complication is that since the cloud particle sizes also increase in a stronger convection system (Jiang et al., 2011), the aerosol-induced convective invigoration likely balances the reduction of cloud particle sizes due to the Twomey effect. The second indirect effect varies with the cloud type and ambient conditions, such as relative humidity, vertical wind shear, and convective potential energy (Lee et al., 2008; Tao et al., 2012; Fan et al., 2016). In cold clouds, aerosols act as IN and increase the number of ice crystals (Sassen et al., 1995; Ström and Ohlsson, 1998). Via the Wegener–Bergeron–Findeisen process, ice crystals grow at the expense of liquid droplets through vapor deposition (Rogers and Yau, 1989), as well as through the processes of riming, aggregation, and accretion (Mitchell et al., 1990). It is still uncertain whether this leads to an enhanced greenhouse effect or a reduction of solar radiation by brighter clouds (Sassen et al., 1995; Lee et al., 2009).

The impact of aerosols on precipitation and cloud macrophysics is even more complex and diverse, representing the least understood component of the aerosol effects (Koren et al., 2012; Rosenfeld et al., 2014; Wang et al., 2014a). Recent studies suggest that the impact of aerosols on precipitation depends on the type of clouds and the environmental conditions in which clouds form (Khain, 2009; Li et al., 2011; Lin et al., 2016). In addition, Li et al. (2008) showed that the aerosol effect is non-monotonic for convective cloud, i.e., an initial enhancement at low aerosol concentrations but a suppression at high aerosol concentrations for precipitation, updraft speed, and cloud fraction. Tao et al. (2007) also showed a switch of aerosol effects on convective clouds, from suppression to enhancement, in different locations.

It is critical to examine the aerosol effects on different cloud types under various weather systems. Numerous previous modeling studies have been devoted to understanding the physical mechanisms of the aerosol effects. However, most of those studies only dealt with either the aerosol direct or indirect effect and focused on a certain cloud type (Wang et al., 2013a). The present study aims to investigate both aerosol radiative and microphysical effects jointly and individually, and quantify the overall aerosol effects on different cloud regimes. Another objective of this modeling study is to explicitly assess the monotonicity in the aerosol–cloud–radiation relationships. Specifically, this study explores the monotonicity of cloud responses to aerosol variations under different cloud regimes, which has profound implications for parameterizations of aerosol–cloud relationships in global climate models.

2. Experimental setup

2.1. *Model description*

In this modeling study, the cloud-resolving Weather Research and Forecast (WRF) model, version 3.1.1, is used. A two-moment bulk cloud microphysical scheme and a modal aerosol scheme were implemented (Li et al., 2008; Wang et al., 2011) to account for the aerosol–cloud–radiation interactions. The two-moment bulk cloud microphysical scheme includes the mass mixing ratio and number concentration for five hydrometeor types—cloud droplets, raindrops, ice crystals, snow, and graupel. The size distribution for each of the five hydrometeors is determined via the gamma function (Li et al., 2008), and 32 microphysical processes are considered, including an explicit condensation calculation using supersaturation and an autoconversion scheme based on relative dispersion (Liu and Daum, 2004). There is no chemistry component in our model.

The Goddard radiation scheme was modified (Fan et al., 2008; Wang et al., 2014b) to include the radiative forcing by the aerosol direct/semi-direct effects. The aerosol module determines aerosol radiative properties, including optical depth, asymmetry factor and single scattering albedo, as a function of wavelength, composition, mixing state, and relative humidity. To enhance the computational efficiency, a lookup table is developed for the optical properties for all size ranges once the aerosol radiative properties are determined.

For each model run, three nested two-way domains are used (Fig. 1a), with spatial resolutions of 18, 6 and 2 km, and a 12-s temporal resolution. The innermost domain is roughly 350 km by 350 km, with 50 vertical levels, and centered at (36.6°N, 97.5°W), covering the same domain as the US Department of Energy Atmospheric Radiation Measurement (ARM) Southern Great Plains (SGP) site near Ponca City, Oklahoma. All model data analyzed in this study are from the innermost 2-km domain with 15-min output intervals. The North American Regional Reanalysis data are used for the initial and boundary meteorological conditions.

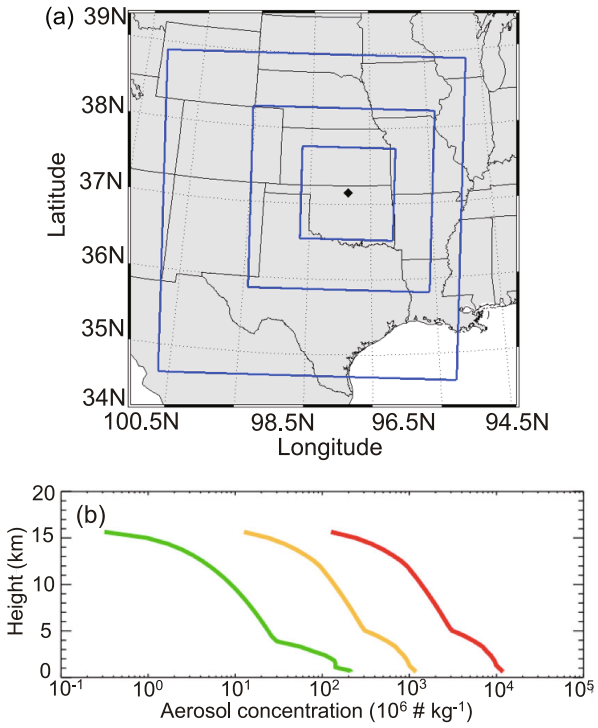

Fig. 1. (a) The three nested domains (blue boxes) used in the WRF model in this study. The innermost domain has a spatial resolution of 2 km. The diamond represents the ARM SGP Central Facility. (b) The three vertical aerosol profiles used in this study: clean (green); SGP (yellow); polluted (red).

2.2. *Aerosol profiles*

To study the aerosol direct and indirect effects and to obtain the monotonicity of the cloud responses, three different aerosol profiles are utilized in this study to represent clean, moderate and polluted environments, respectively (Fig. 1b). The two types of anthropogenic aerosols mainly considered in this study are sulfates and black carbon. The clean cases use a relatively clean background continental profile with an initial surface aerosol number concentration of 210 cm^{-3}, as used by Li et al. (2009) from the Texas Air Quality Study 2000 campaign. The moderate cases, herein referred to as SGP cases, are based on aerosol measurements taken at the SGP site during the 2003 Aerosol Intensive Observation Period (IOP) campaign. The SGP cases have an initial surface concentration of 1200 cm^{-3}. The polluted cases have an initial surface concentration that is 10 times greater than the SGP profile, at 12000 cm^{-3}, which is a similar magnitude to the urban case used by Cheng et al. (2007). For all three profiles, the aerosol concentration is assumed to decrease exponentially with height above about 5 km (Cheng et al., 2007; Li et al., 2009). As aerosol mass and number concentrations are prognostic variables in the model, aerosol vertical mixing and horizontal advection are explicitly considered. There is no direct emission of aerosols from the surface, but aerosols can be advected into the inner domains from the boundaries under favorable wind conditions. Aerosols are removed by nucleation scavenging. Internal mixing of 95% sulfate and 5% black carbon by mass is assumed for studying radiative effects of light-absorbing aerosols. Such a composition assumption for the calculation of radiation has been justified by previous field measurements (Levy et al., 2013) and a modeling study (Wang et al., 2014b) in the southern United States. Each aerosol profile will be used for the simulations with the aerosol direct and indirect effects (DIE) and the simulations with the aerosol indirect effect only (IEO).

2.3. *Case studies*

During 1–26 March 2000 the Cloud IOP campaign was conducted at the ARM SGP site. The goal of the campaign was to collect three-dimensional cloud properties from observational data including the standard set of ARM SGP instruments, radar and lidar observations, and aircraft measurements, which included a total of 12 flights during the period. The cloud data has been divided into six subperiods (A through F) that contain different synoptic and cloud properties, and have been extensively studied regarding cloud–climate feedback in atmospheric general circulation models (Zhang et al., 2005). For this study, aerosol–cloud interactions will be studied for three of the six subperiods (hereafter denoted as A, D and E, for convenience).

Case A pertains to clouds to the north of a developing low-pressure system from 1500 UTC 1 March to 0000 UTC 5 March 2000 (Fig. 2a). About 10 h prior to the start of this case, a cold front moved through the domain at about 0430 UTC 1 March. Clouds began to move into the domain from a low-pressure system that formed in the Four Corners region at around 2000 UTC 1 March. By 2000 UTC 2 March, the low-pressure system had entered the southwest corner of the domain, while a thick layer of cloud covered the region. Between 2 and 3 March, the center of the low moved along the Oklahoma–Texas border, with cloud development primarily to its north. By 1330 UTC 3 March, the system had left the region, with the skies mainly clearing up by 1200 UTC 4 March as a high-pressure system kicked in.

Case D pertains to a collection of less-precipitating clouds, i.e., a series of stratus from 2100 UTC 11 March to 1200 UTC 14 March 2000 (hereafter referred to as Case D1) and shallow cumulus from 1200 UTC 14 March to 1200 UTC 15 March 2000 (Case D2). Prior to the start of this case, there was a stationary front to the south draped across central Texas from the Louisiana–Missouri border across to New Mexico, with a high-pressure center behind it located centrally over the domain. During 13 March, a cold front passed to the north of the domain, which also moved the high-pressure center out of the region. During 14 March, a weak low-pressure system passed through southern Texas, facilitating some shallow convection and light precipitation in Oklahoma (Fig. 2b). To better understand the aerosol effects on different types of cloud, our analyses will be conducted on the two periods separately.

Case E pertains to clouds associated with the genesis of a cold front that moved through the domain from 0900 UTC 15 March to 0000 UTC 20 March 2000 (Fig. 2c). The cold front approached from the north-northwest and arrived in the do-

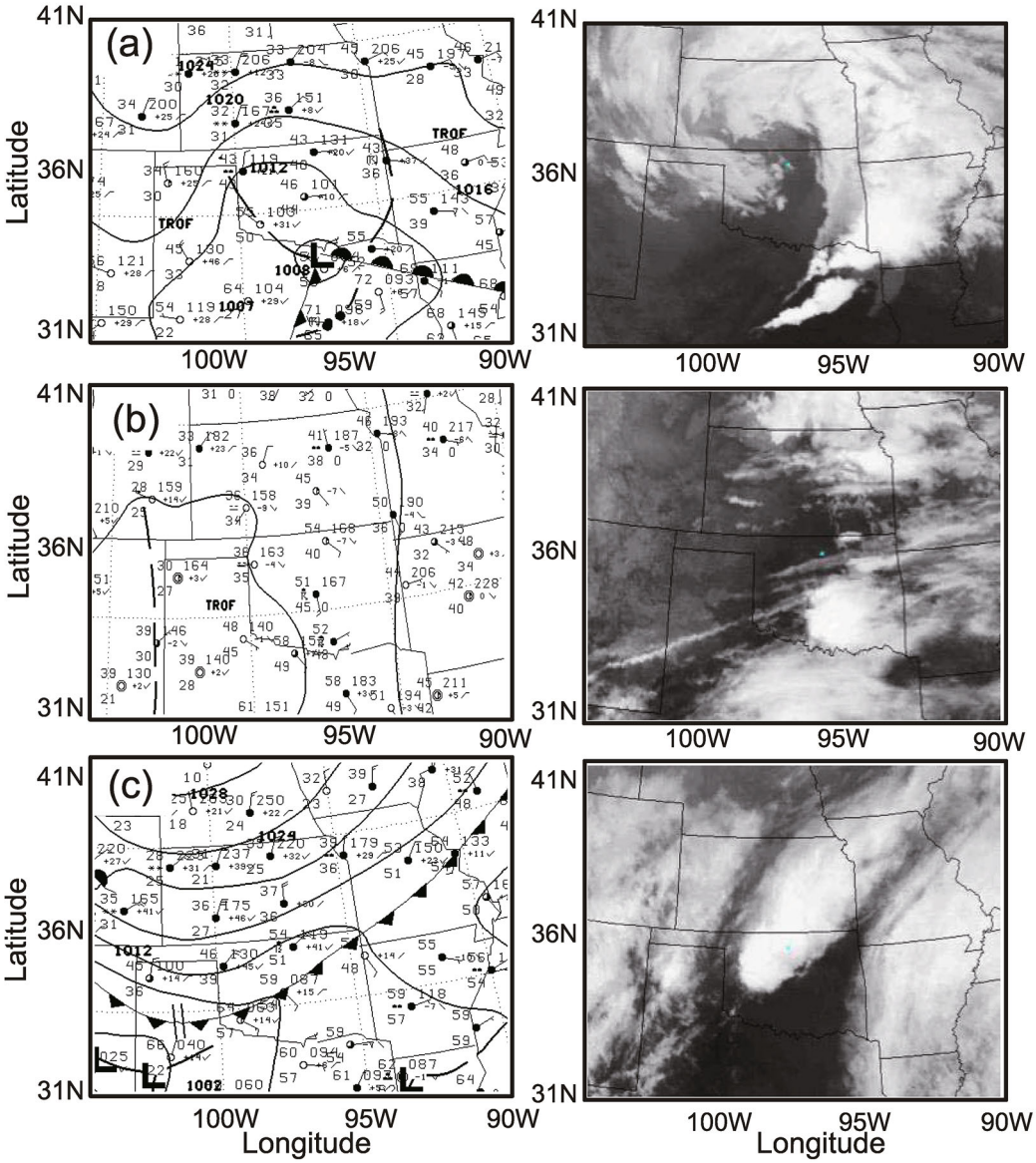

Fig. 2. Surface pressure and wind maps (left) and satellite images (right) for each of the three cases in this study: (a) 0300 UTC 3 March 2000 (low-pressure system); (b) 1200 UTC 14 March 2000 (non-precipitating stratiform); (c) 0300 UTC 16 March 2000 (cold front). Satellite images were taken 15 min before the listed times.

main at about 0100 UTC 16 March. Satellite imagery shows convective development directly over the SGP central facility from 0000 UTC to 0300 UTC. By 1300 UTC the cold front had moved south into Texas and out of the domain, whereupon it stalled. Behind the cold front, mainly lower-level clouds persisted over the domain due to an upper-level low. On 18 March, another low-pressure system passed to the south of the domain right long the Oklahoma–Texas border. The region finally cleared out by about 2000 UTC 19 March.

3. Results and discussion

3.1. *Microphysical properties of hydrometeors*

Distinct microphysical responses to aerosol initial conditions are shown for all the three cases and vary with the microphysical parameters of interest and depend on cloud types. Regardless of whether we look at the heavy-precipitation cases (Case A and Case E) or the case dominated by less-precipitating clouds (Case D), our IEO simulations show that all cloud droplet microphysical properties, including mass mixing ratio, number concentration and effective radius, monotonically change with aerosols, indicating a relatively straightforward role played by CCN in determining the cloud microphysical properties. Regardless of whether or not the aerosol radiative effect is included, the number concentration of cloud droplets increases strictly as a function of CCN available for water vapor condensation in each case (Figs. 3a, d, j and i), and such rates of increase are about the same as the aerosol elevation rate we impose in the experiment. The cloud droplet mass content also increases monotonically along with the elevation of aerosol concentration,

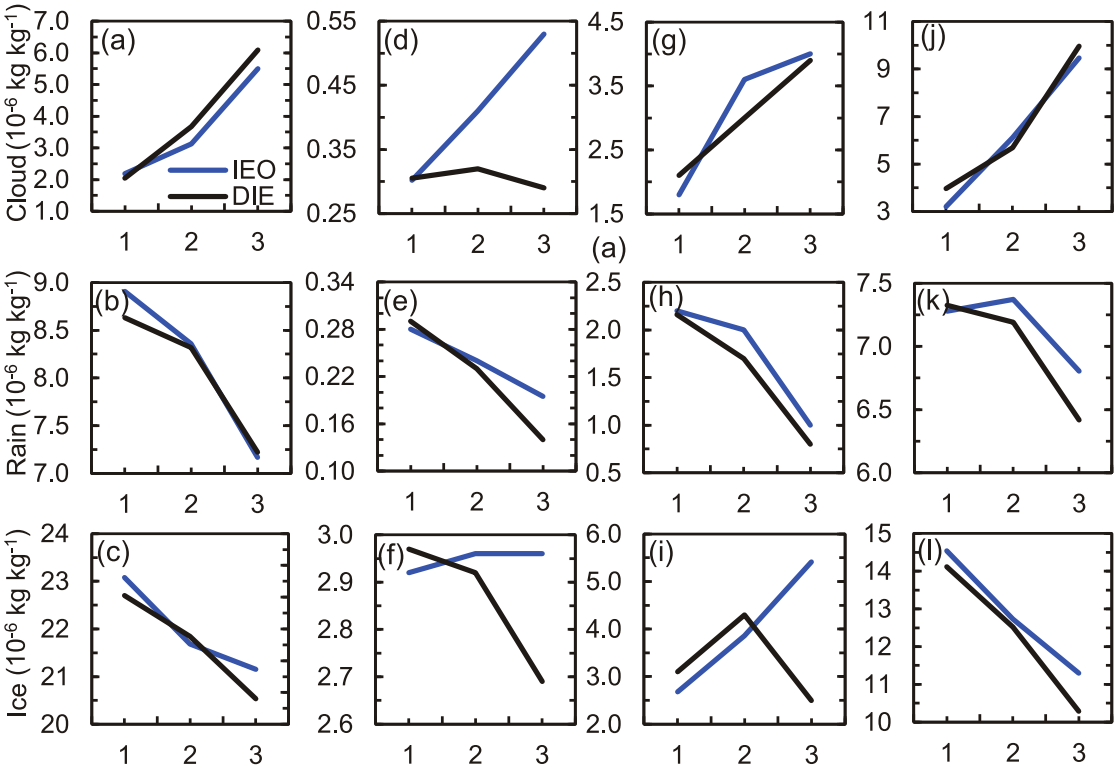

Fig. 3. Domain-averaged water mixing ratios of cloud (upper row), rain (middle row), and ice hydrometeors (lower row) for (a–c) Case A, (d–f) Case D1 (stratus period), (g–i) case D2 (cumulus period), and (j–l) Case E, with the numbers 1, 2 and 3 representing the clean, SGP, and polluted aerosol profiles, respectively. The black lines indicate the DIE cases and the blue lines the IEO cases.

except for the stratus clouds in Case D1 when aerosol radiative effects are included (Fig. 3d). A significant reduction in droplet mass concentration by the aerosol radiative effect is found in Case D1. Overall, inclusion of aerosol radiative effects in simulations (DIE cases) has limited influence on the trend of cloud droplets but shows some impacts on the magnitude, particularly for the less-precipitating-cloud dominant case (Case D).

To understand the aerosol radiative influence, we show the air temperature changes under different aerosol conditions between DIE and IEO in Case D (Fig. 4). With the increase in the aerosol concentration from the clean to polluted conditions, the variations in air temperature due to aerosol radiative effects become larger. Under the polluted conditions (Fig. 5c), there is a significant warming in the lower free troposphere from Day 72 to 74. This can further induce a reduction in relative humidity and a decrease in cloud content, as shown in Fig. 3, which is the canonical semi-direct effect. Meanwhile, the warming in the free troposphere and cooling inside the boundary layer form a temperature inversion and inhibit convection and vertical mixing. Such a thermodynamic effect also contributes to cloud reduction when the aerosol radiative effects are considered in DIE. Another interesting phenomenon is that the altitude of the warming center is elevated from noon throughout the afternoon, indicating the aerosols are lifted upward along with the heated air parcel in the non-precipitating environment.

Both the mass mixing ratio and number concentration of raindrops exhibit a decreasing trend in response to aerosol for all three cases (Figs. 3 and 4). This is attributable to the smaller cloud droplets under polluted conditions, which are not conducive to collision/coalescence in the production of raindrops. Figures 6a–c show the cloud droplet effective radii are reduced at all cloud points within the cloud ensembles in all three cases from the clean to the polluted conditions. The size of raindrops is a key factor controlling the precipitation amount at the surface, but its response to aerosol perturbation is more complicated than those from raindrop mass and number concentrations. By only considering the CCN effect in IEO, the increase in raindrop size is found at most times and levels in the three cases (Figs. 6d–f); however, some scattered reductions in raindrop size occur, possibly due to the changes in ice-phase particle (e.g., snow, graupel) size, as well as convective strength.

Different from cloud droplets and raindrops, ice particles exhibit some non-monotonic responses in different cloud regimes, especially for the less-precipitating stratus and cumulus. Relative to the clean profile, the mass mixing ratio of ice crystals is reduced in the polluted profile by 7% and 40% for Case A and Case E, respectively. The number concentration of ice crystals generally increases as aerosol increases (Fig. 4), so their effective radius decreases by varying degrees. The vertical profiles of the ice particle size change show most of the radius reductions occur in the upper part

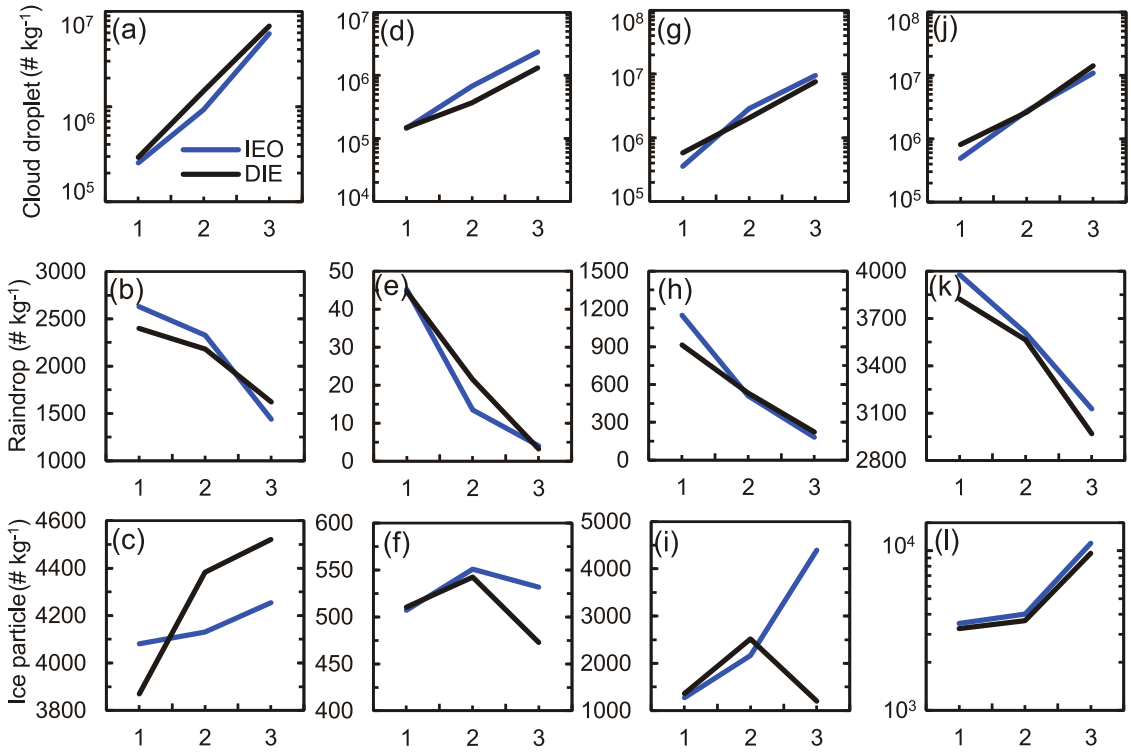

Fig. 4. Domain-averaged number concentration of cloud (upper row), rain (middle row), and ice hydrometeors (lower row) for (a–c) Case A, (d–f) Case D1, (g–i) Case D2, and (j–l) Case E, with the numbers 1, 2 and 3 representing the clean, SGP, and polluted aerosol profiles, respectively. The black lines indicate the DIE cases and the blue lines the IEO cases.

of the cloud systems (Figs. 6g–i), while lower-level ice crystals can even grow bigger at the expense of more supercooled droplets. Similar to cloud and raindrops, the aerosol radiative effect in DIE does not change the trend of ice crystals in response to increases in aerosol concentration, but it does alter the absolute concentrations of the hydrometers for the two precipitating cases (Case A and E) compared with IEO. In particular, the number concentration of ice crystals is greatly enhanced in DIE simulations at high aerosol levels in Case A (Fig. 4c). For the stratus in D1, the CCN effects on ice mass and number concentrations are either saturated or reversed from the moderate to heavy polluted conditions. Through comparison of DIE and IEO in Figs. 4 and 5, it appears that both the monotonicity of the microphysical response and the magnitude of the microphysics of ice crystals could be greatly modulated by aerosol direct effects in Case D.

3.2. *Precipitation*

Figure 7 presents the evolution of rain rates throughout Case A. The simulated temporal variation of rain rates generally agrees with the observations based on rain gauge data from the Arkansas Red-Basin River Forecast Center (ABRFC). For example, both simulations and observations show intensive precipitation started from 0900 UTC on Day 62 and ended around noon on Day 63. However, the primary peak during the first precipitation period is delayed by half day in the simulations, possible due to the bias in the simulated storm center. The strongest updrafts are observed during the first period, suggesting a convective origin of precipitation. For both the DIE and IEO cases, the aerosol concentration and accumulated precipitation are positively correlated, consistent with the larger size of raindrops under the more polluted conditions. The larger raindrops could have a higher chance to survive evaporation when they precipitate out from clouds, leading to more surface precipitation. There is a statistically significant difference between rainfall amounts with and without the direct effect. More precipitation is produced in the IEO case than in the DIE case for both the clean and polluted profiles, which indicates that through blocking more radiation into the atmosphere, the aerosol direct effect systematically weakens the convection strength associated with the cloud development [Fig. S1 in electronic supplementary material (ESM)].

Mid-level non-precipitating clouds are primarily present during most of Case D, but some shallow cumulus clouds were formed to the south of the SGP near the end of the period, bringing a brief period of light precipitation, based on the ABRFC observations (Fig. 7c). Our model produces some light precipitation at different times during the "non-precipitation" stratus D2 stage according to the observations. The intensive precipitation in the simulations also comes from the convective event in D2, but the rain rates are generally overestimated by a factor of two compared to the observed values. Both observations and simulations show

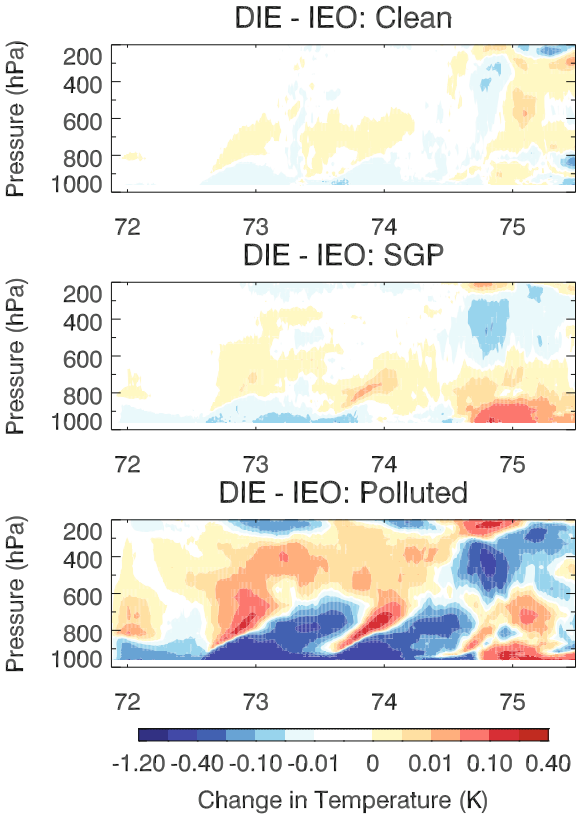

Fig. 5. Vertical–temporal profiles of domain-averaged air temperature changes due to aerosol radiative effects under three aerosol concentrations for Case A. *x*-axis indicates day of the year.

that the convective event is the only period with significant rainfall and is the main contributor to the accumulated rainfall, so the total accumulated rainfall responses in Fig. 7d reflect the changes in D2. Both the DIE and IEO cases generally show similar non-monotonic precipitation trends in response to aerosol, i.e., the accumulated precipitation is enhanced from the clean profile to the SGP profile, and is then further reduced in the polluted profile. The nonlinearity of the relationship between precipitation and aerosol can be explained by the corresponding nonlinearity of the microphysical effects of aerosol on shallow cumulus clouds. At the relatively low aerosol levels (from clean to SGP), the mass mixing ratio of raindrops decreases by 10% (Fig. 3h), which is much smaller than their 58% reduction in number concentration (Fig. 4h). This leads to a relative increase in the effective radius of raindrops, and hence the raindrops have a better chance to survive through the under-saturation below clouds, resulting in an enhancement in surface precipitation from the clean to the SGP profile. However, due to the larger amount of smaller cloud droplets, warm rain is suppressed in the polluted profile by less efficient collision/coalescence processes. Significant differences in magnitudes of precipitation exist between the DIE and IEO cases at high aerosol levels (SPG and polluted). The largest difference between the DIE and IEO model runs is in the polluted profile in the IEO case, which has 43% more rain than the DIE case on average. The higher amounts of precipitation in the IEO cases can be traced to the higher amounts of cloud, rain and ice water in IEO than in DIE (Fig. 3), and this is also consistent with the weaker convection during the period with shallow cumulus cloud in DIE (Fig. S2). By including the direct effect in the DIE cases, absorbing aerosols may reduce the instability by slightly warming the atmosphere, thereby reducing cloud and precipitation formation. This is evident in Fig. 4 insofar as that by contracting the DIE and IEO cases, the temperature changes are positive in the atmosphere during daytime and negative at the surface, suggesting that absorbing aerosols in the DIE cases warm the atmosphere considerably and cool the surface correspondingly, thereby weakening the convection, reducing the atmospheric instability, and suppressing cloud and precipitation formation.

During Case E, the model does relatively well in predicting the timing of four maxima of precipitation in comparison to observational data, but somehow underestimates the precipitation amount before Day 78 and overestimates it after Day 79 (Fig. 7e). The first precipitation maximum was from about 0000 to 1200 UTC on Day 76, corresponding to the strongest period of convection associated with the passage of the cold front. Precipitation during this period shows a non-monotonic response to initial CCN concentrations, as the peak values of rainfall rates during this period are 1.27, 1.31 and 1.13 mm h^{-1} for the clean, SGP and polluted aerosol profiles with IEO, respectively. Such non-monotonicity was also found in the CCN effects on a cumulus cloud by Li et al. (2008). The next two precipitation maxima occurred during the stratiform rain event from about 1200 UTC on Day 76 to 1000 UTC on Day 78, throughout which very few ice particles were present (Fig. S3), and there was generally a linear relationship between the aerosol concentration and rain rates. The final two precipitation maxima, from about 1200 UTC on Day 78 to 1400 UTC on Day 79, are associated with another convection event. The response of the rainfall rates to aerosol during this period is a little complicated, as the last precipitation maxima on Day 79 are 0.75, 0.64 and 0.72 mm h^{-1} from the clean, SGP, to polluted aerosol profiles. The largest contributor to the accumulated precipitation for Case E is due to convective sources on Day 76; hence, the overall trend of precipitation in response to aerosols is first and increase and then a decrease. When comparing the accumulated precipitation between the DIE and IEO cases, statistically more precipitation (about 1–2 mm on average) is produced in the IEO cases than in DIE cases. The higher precipitation for the IEO cases could be attributed to the larger amounts of rain and ice water available.

3.3. *Cloud fraction*

Figure 8 shows the simulated and observed cloud fraction, defined as the fractional area percentage of clouds in an atmospheric layer. Observations were obtained at the SGP Central Facility using the Active Remote Sensing of Clouds Value-Added Product. The modeled cloud fraction is averaged over the 25 nearest grid points (a five-by-five horizontal box around the SGP Central Facility) with a total water mix-

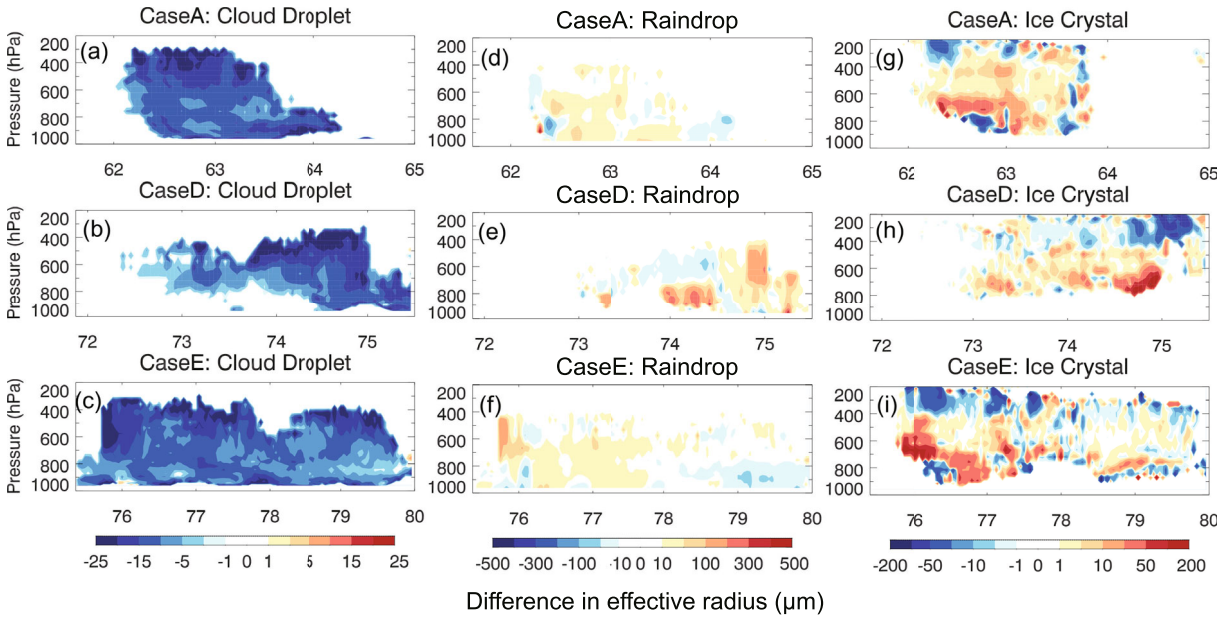

Fig. 6. Vertical–temporal profiles of changes in the effective radius of (a–c) cloud droplets, (d–f) raindrops, and (g–i) ice crystals, between the clean and polluted conditions, for Case A (upper row), Case D (middle row), and Case E (lower row). Only IEO results are shown here.

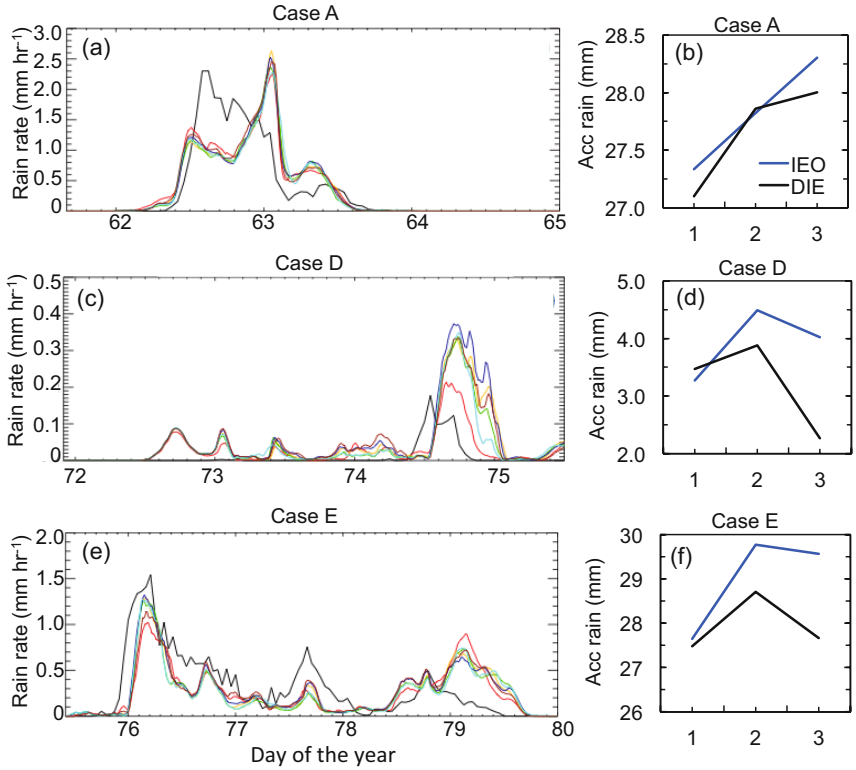

Fig. 7. Temporal evolution of observed and simulated rates (left-hand panels) and accumulated precipitation (right-hand panels) for (a, b) Case A, (c, d) Case D, and (e, f) Case E. Plotted colors correspond as follows: black—observed; green—clean DIE; yellow—SGP DIE; red—polluted DIE; cyan—clean IEO; blue—SGP IEO; dark red—polluted IEO. In the right-hand panels, the numbers 1, 2 and 3 represent the clean, SGP, and polluted aerosol profiles, respectively. In the left-hand panels, the black lines indicate the DIE cases and the blue lines the IEO cases. Significant at the 95% confidence level.

ing ratio (Q_{tot}) greater than 10^{-6} kg kg^{-1}, where Q_{tot} is the sum of the cloud, ice, snow, and graupel water mixing ratios.

In Case A, as a developing low-pressure system passed to the south of the domain along the Oklahoma–Texas border, a few different cloud types—primarily cumulus and stratus clouds—passed through the domain. The general evolutions of cloud fraction are comparable between the simulations and the observation, with two distinct periods of deep convection and a long period of low-level clouds. The DIE induces an increase in cloud fraction in both convective clouds and stratiform clouds from clean to polluted conditions (Fig. 8a). The overall cloud fraction during the entire case in Fig. 8 shows that with the elevated aerosol concentrations, the cloud fraction has a fractional increase of 16.6% for DIE and a decrease of 4.6% for IEO. The non-monotonic responses of cloud fraction to different aerosol concentrations in the IEO of this case reveal that cloud fraction may not be a good indicator of the aerosol invigoration effect discussed in the previous sections. The cloud fraction changes due to aerosols can be largely buffered by the interactions between clouds and ambient air, as the entrainment rate can be modulated after the stronger convection along with the aerosol invigoration effect. One good example is the reduction of relative humidity for the trade wind cumulus in the subtropics (Seifert et al., 2015). Those competing factors make the change in cloud fraction highly mutable after the aerosol perturbation.

Most of the clouds in Case D are mid-level non-precipitating clouds, some of which contain ice particles. Near the end of the case, some shallow cumulus clouds occurred to south of the SGP Central Facility. Observations show there were primarily two periods of non-precipitating clouds at around 0000 UTC on Day 73 and 74, and a short-lived convective cloud late on Day 74 (Fig. 8). The simulated clouds in the two periods are generally larger and thicker than observed. The cloud fractions in six experiment runs show close resemblance (Fig. 8). The major differences are the reduction in cloudiness at about 0700 UTC on Day 73, and at about 1800 UTC on Day 74. Only the aerosol radiative effect emerges in both D1 and D2, showing a negative correlation between aerosol and cloud amount, while the changes

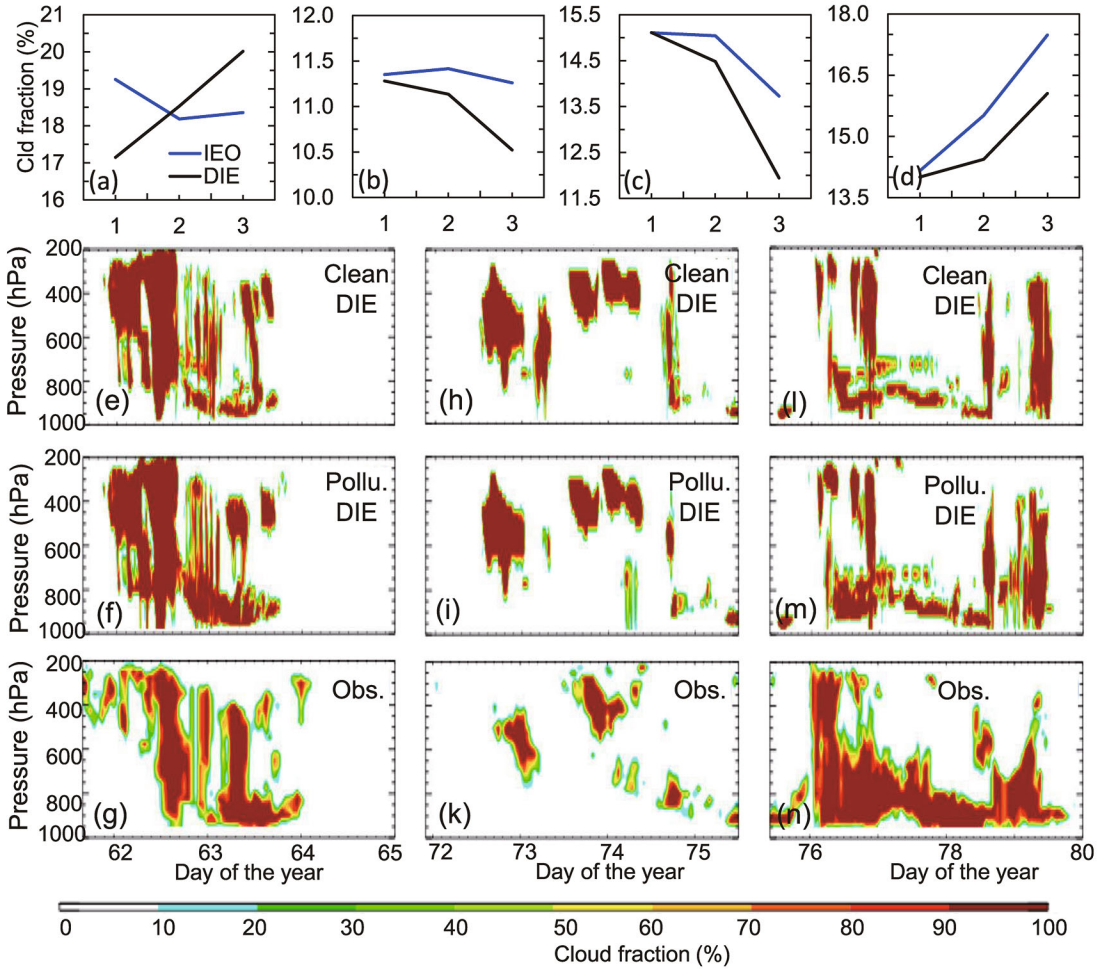

Fig. 8. Simulated and observed cloud fraction for Case A (left-hand panels), Case D (middle panels), and Case E (right-hand panels): (a–d) average cloud fraction over the entire period, in which the numbers 1, 2 and 3 denote the clean, SGP, and polluted aerosol profiles, respectively; (e, h, l) clean DIE simulations; (f, i, m) polluted DIE simulations; (g, k, n) observations.

in cloud fraction in IEO are insignificant in D1. The cloud fraction can be reduced by 20% due to aerosols in the DIE of Case D2.

Cloud cover was continuously present over the SGP domain during Case E, primarily due to a cold front, two-day trailing stratiform clouds, and another low-pressure system on the last day. Generally, the model produces thinner cloud depth but consistent evolution compared to the observations (Fig. 8). The lower simulated cloud fraction is partly due to the exclusion of the rainwater mixing ratio in calculating the cloud fraction. Actually, when the rainwater mixing ratio is included, the modeled cloud fraction appears exceptionally thicker than observed. This is the same reason for the biased liquid water path (LWP) simulations in the next section. The overall cloud fraction throughout Case E increases with higher aerosol concentrations for both the DIE and IEO cases (Fig. 8), with a relative increase of 14.8% and 23.8%, respectively. For the DIE cases, during the cold frontal passage on Day 76, with increased aerosol concentrations, there is an increase in lower-level clouds, but a decrease in deep convective clouds is observed. During the Day 79 low-pressure system period, the cloud fraction significantly increases. For the IEO cases, with respect to increasing aerosol concentration, the cloud fraction increases during each of the three periods of note. Also during all three periods, IEO has a larger increase in cloud fraction than that in DIE.

3.4. *LWP*

The response of the LWP to CCN perturbations is directly related to the aerosol indirect forcing, but the simulated relationships from different climate models do not converge (Fan et al., 2016). The semi-direct effect of absorbing aerosols further complicates the relationship between aerosols and the LWP (Lin et al., 2016). In both Case A and E, the simulated LWP exhibits a robust monotonic increase along with the elevation of aerosol loading, due to the CCN effect. Comparing the clean and polluted scenarios, the LWP can be enhanced by 50% to 75% in Case A and E. Such a relationship is not subject to the aerosol radiative effect for the convective cloud regime, as LWP changes are about the same between DIE and IEO for Case A and E. For Case D, which has an overall smaller liquid cloud amount than Case A and E, the variations of LWP are strongly influenced by the radiative effect of light absorbing aerosols (Fig. 9). The heating in the free troposphere induced by aerosols can reduce the LWP of the stratus by 25% in the polluted scenario during Case D1, and even reverse the trend of LWP responses to aerosols from positive to negative. Similarly, for the cumulus in D2, the LWP is reduced by about 20% when comparing DIE and IEO for both moderate and heavy polluted aerosol conditions.

3.5. *Radiative fluxes and surface temperature*

In all three cases, the modeled shortwave radiation reaching the surface shows a monotonic decrease by increasing aerosols, while the magnitude of the decrease depends on cloud type and is affected by the aerosol radiative effect. For the IEO cases, the general reduction in shortwave radiation agrees with the monotonic increase in LWP but decrease in cloud droplet radius. By considering the aerosol direct effect, Case A and D show a much larger reduction in surface shortwave radiation, by as much as -30 W m^{-2} (Fig. 10). In contrast, due to the thick cloud layer in Case E, the aerosol radiative effect on the surface radiation is not evident for both the clean and polluted conditions. On the other hand, we find that the cooling from the aerosol indirect effect is most significant in Case E, which has greater cloud thickness and more persistent low-level stratiform cloud than Case A and D. Comparing the aerosol-induced trends of shortwave radiation

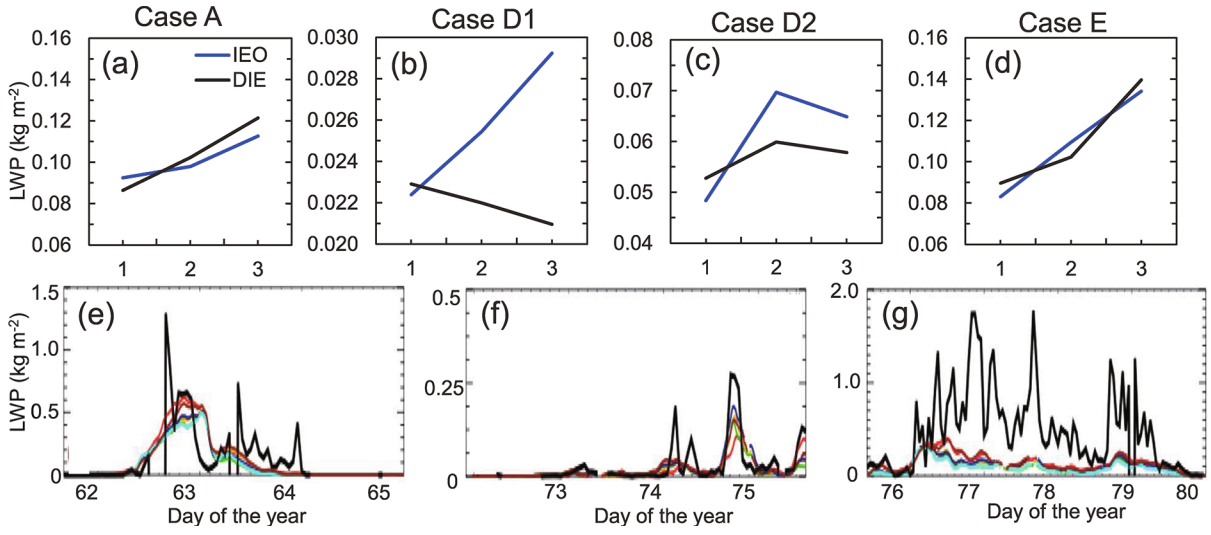

Fig. 9. Simulated and observed LWP for (e) Case A, (f) Case D, and (g) Case E. Upper row: averaged over the entire period and the innermost domain, in which the numbers 1, 2 and 3 denote the clean, SGP, and polluted aerosol profiles, respectively. Lower row: averaged for the entire domain, in which the plotted colors correspond as follows: black—observed; green—clean DIE; yellow—SGP DIE; red—polluted DIE; cyan—clean IEO; blue—SGP IEO; dark red—polluted IEO; lavender—observations.

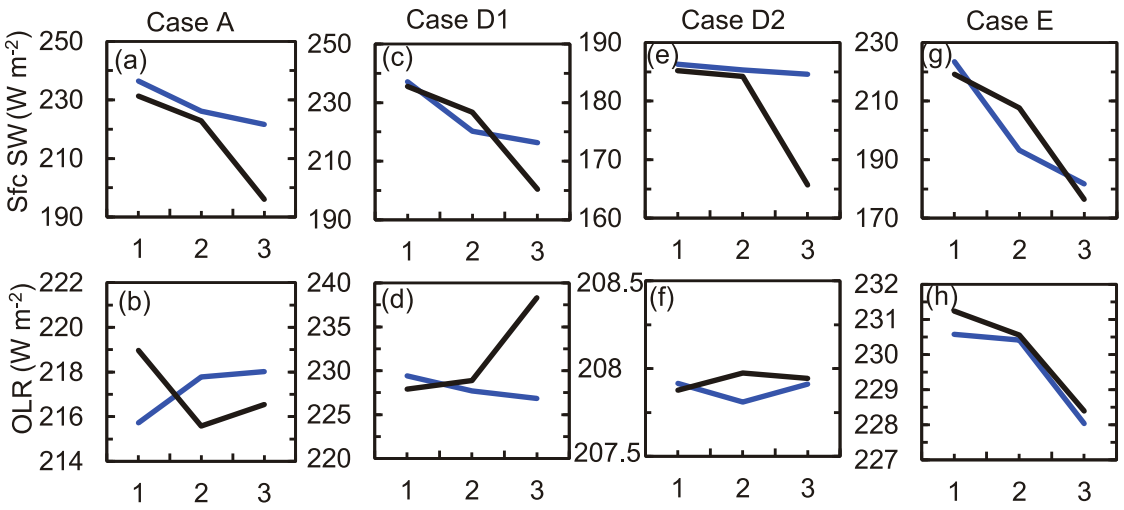

Fig. 10. Simulated surface downwelling shortwave radiation fluxes (upper row) and TOA OLR (lower row) for (a, b) Case A, (c, d) Case D1, (e, f) Case D2, and (g, h) Case E. The numbers 1, 2, and 3 denote the clean, SGP, and polluted aerosol profiles, respectively.

in the IEO runs among the three cases, Case E exhibits the largest reduction in shortwave radiation by increasing CCN.

The response of outgoing longwave radiation (OLR) at the TOA to aerosol variations is modulated by the overall cloud fractions. Such a hypothesis can be verified by comparing the responses of OLR (Fig. 10) and cloud fraction (Fig. 8). It is found that almost all the trends of OLR are opposite to those in cloud fraction, as the OLR (cloud fraction) decreases (increases) in the DIE of Case A, IEO of Case D, and both the DIE and IEO of Case E, but increases (decreases) in the IEO of Case A and DIE of Case D1. A quantitative analysis of the co-variations of cloud fraction and OLR in Fig. 11 shows that the correlation coefficient between these two quantities is greater than 0.8. This good agreement reinforces the fact that clouds play a crucial role in altering the Earth's radiative budget regionally and globally. Comparing the DIE and IEO cases, the aerosol radiative effect can even change the sign of the OLR response. For example, in Case A, introducing aerosol–radiation interactions results in a change of OLR due to aerosols from +2.4 to −2.4 W m^{-2}. Even though the cloud top height is another factor that can potentially alter the OLR, we find the cloud top heights do not significantly change for different aerosol conditions in all three cases, as evidenced by the vertical profiles of cloud fraction (Fig. 8) and ice water content (Fig. S3).

Surface temperature changes closely follow the surface radiation imbalance. The model-simulated surface temperature shows good agreement with surface station measurements at SGP. In Case A and D, only aerosol radiative effects in the polluted scenario stand out and produce a surface cooling (Fig. 12). The insignificant surface temperature response in IEO can be attributed to the cancellation between both enhanced shortwave cooling and longwave warming at the surface. In contrast, the surface cooling induced by aerosols is significant in both the IEO and DIE of Case E. Overall, the responses of surface temperature to aerosol variations are

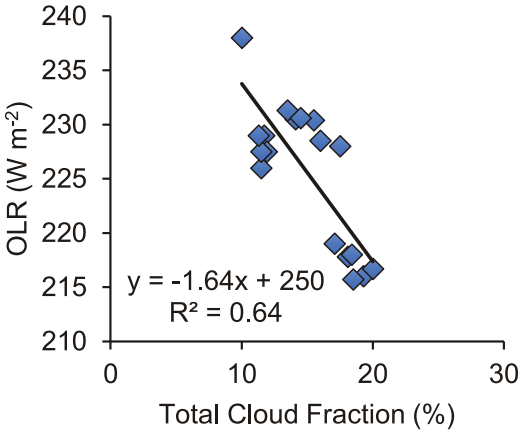

Fig. 11. Correlation between total cloud fraction and OLR from three cases under different aerosol conditions.

highly similar to those of downwelling shortwave radiative fluxes at the surface (Fig. 10).

4. Conclusion

The individual mechanisms of aerosol–cloud interaction in certain types of cloud have been extensively examined in previous studies using similar cloud-resolving models. However, the aerosol effects on cloud ensembles where multiple types of clouds coexist in the real atmosphere receive much less attention. In this study, we adopted an "ensemble" approach and compiled three cases that were well observed over the same region (US SGP) during the same season (springtime). An aerosol-aware WRF model was used to explore the differences in the responses of cloud micro- and macrophysics, precipitation, and radiation, to aerosol perturbations in the complex continental cloud systems. The model employs a two-moment bulk microphysics scheme to account

for the aerosol microphysical effect, as well as a modified Goddard radiation scheme to simulate the aerosol radiative effect. Three different cloud systems during the March 2000 Cloud IOP campaign at the ARM SGP site were examined, including: a low-pressure system, less-precipitating stratus and shallow cumulus, and a cold front. The impacts of increasing the aerosol concentration were quantified, and the aerosol radiative (direct and semi-direct) and microphysical (indirect) effects compared. Our cloud-resolving simulations generally captured the major features of the observed temporal variations in precipitation for all three cases.

The sensitivity experiments showed that the distinct microphysical responses of cloud collections to initial aerosol loadings depend highly on the cloud types and synoptic conditions. For the convective cases with moderate-to-heavy precipitation, the microphysical properties for hydrometeors showed robust monotonic trends in response to aerosol loadings, evident in the dependences of the mass content and number concentration of cloud droplets and rain drops on aerosols. The inclusion of aerosol direct effects in those cases had little influence on the monotonicity of the microphysical response for the heavy precipitating situation. For the less-precipitating stratus clouds, the monotonicity of the microphysical response to aerosols depended on the types of hydrometeors examined, as the cloud water content can be strongly modulated by aerosol direct and semi-effects.

The overall response of domain-averaged accumulated precipitation to aerosol initial concentrations showed a linearly increasing trend for convective cloud, but some tipping points in stratiform or shallow cloud. The monotonicity of the precipitation response to aerosol initial concentrations differed from case to case and varied with cloud types and their evolving stages, indicating a high dependence of the precipitation response on the weather environment in which the cloud systems developed. By comparing the IEO simulations with DIE simulations, the importance of aerosol direct effects emerged, even though the aerosol direct effects did not modify the trends of precipitation in response to aerosol perturbations.

The changes in cloud macrophysics, such as cloud fraction, did not show any similarities to those in cloud microphysics. The responses of cloud fraction to different aerosol concentrations were quite distinct in the different cases. Specifically, in a convective cloud system like case E (Fig. 8d), we found the increase in cloud fraction is due to the increase in liquid cloud mass in the stratiform clouds trailing the deep convection core. In a less-precipitating cloud system like our case D, the absorbing aerosols can heat up the air mass in the cloud layer, cool the air near the surface, reduce the relative humidity in the cloud layer, weaken the turbulence in the boundary layer, and eventually decrease the cloud fraction (Figs. 8b and c). Note that previous reports of the aerosol effects on cloud fraction were mainly derived from cloud-resolving simulations (e.g., Lin et al., 2016), while GCMs always predict little change in cloud fraction in response to aerosols perturbations (e.g., Wang et al., 2015). This emphasizes the importance of cloud fraction parameterizations in GCMs. The LWP exhibited a robust monotonic increase along with the elevation of aerosol loading for convective clouds and their trailing stratiform clouds, while there was no significant change in LWP for the thin mid-level cloud with little water content inside. The modeled shortwave radiation reaching the surface showed a monotonic decrease by increasing aerosols, while the magnitude of the decrease depended on the cloud type and was affected by the aerosol radiative effect. The responses of OLR were closely linked with the total cloud fraction under different aerosol loadings. Ultimately, the surface temperature changes closely followed the

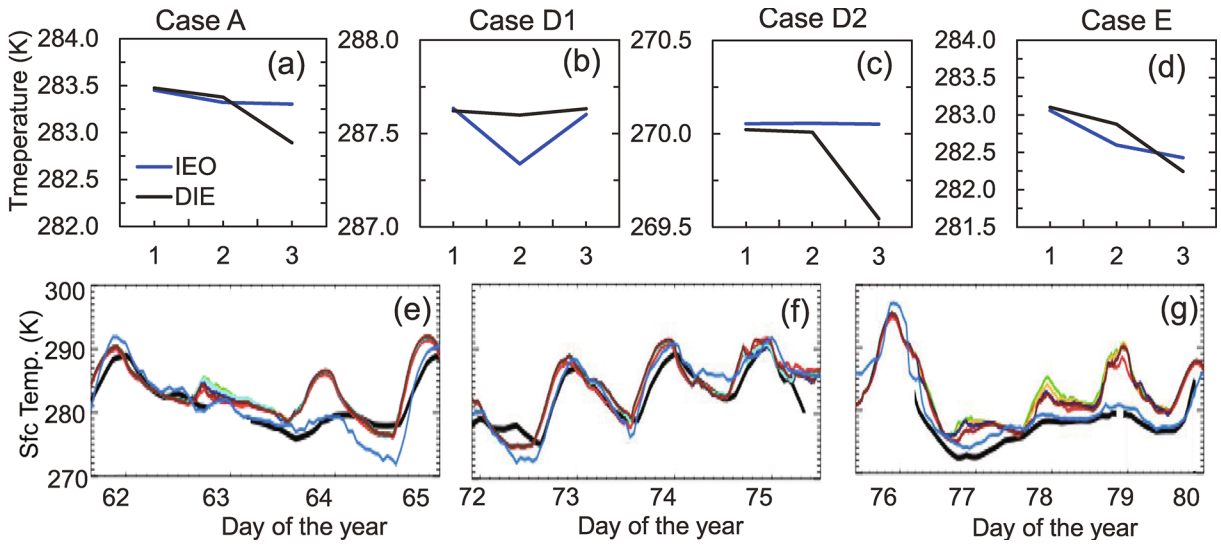

Fig. 12. Simulated and observed surface temperature for (e) Case A, (f) Case D, and (g) Case E. Upper row: averaged surface temperature over the entire period and the whole domain. Lower row: temperature evolution in three cases, in which the plotted colors correspond as follows: black—observed; green—clean DIE; yellow—SGP DIE; red—polluted DIE; cyan—clean IEO; blue—SGP IEO; dark red—polluted IEO; lavender—METAR temperature observations.

surface radiation imbalance, including both shortwave and longwave contributions, but the former carried more weight.

The results from this modeling study highlight the complexity of the aerosol–cloud–precipitation–radiation interactions that vary on a case-by-case basis. In addition, this study has shown that studying the aerosol microphysical effect alone is insufficient to assess the changes of clouds in the real atmosphere, as the aerosol radiative effects can also produce profound impacts on cloud development and precipitation processes. Therefore, long-term, high-resolution model simulations with comprehensive aerosol effects are needed to quantify the climatic effects of aerosols on regional radiation budgets and the hydrological cycle.

Acknowledgements. Dr. Yuan WANG appreciates the funding support provided by NASA ROSES14-ACMAP and NSF (Award No. 1700727). Dr. Yangang LIU is supported by the US DOE ASR program. Dr. Jonathan H. JIANG acknowledges the support of the Jet Propulsion Laboratory, California Institute of Technology, under contract with NASA. All model results are available upon request from Yuan WANG (yuan.wang@caltech.edu).

Electronic supplementary material: Supplementary material is available in the online version of this article at https://doi.org/10.1007/s00376-017-7091-5.

REFERENCES

Ackerman, A. S., O. B. Toon, D. E. Stevens, A. J. Heymsfield, V. V. Ramanathan, and E. J. Welton, 2000: Reduction of tropical cloudiness by soot. *Science*, **288**, 1042–1047, https://doi.org/10.1126/science.288.5468.1042.

Albrecht, B. A., 1989: Aerosols, cloud microphysics, and fractional cloudiness. *Science*, **245**, 1227–1230, https://doi.org/10.1126/science.245.4923.1227.

Cheng, C.-T., W.-C. Wang, and J.-P. Chen, 2007: A modelling study of aerosol impacts on cloud microphysics and radiative properties. *Quart. J. Roy. Meteor. Soc*., **133**, 283–297, https://doi.org/10.1002/qj.25.

Fan, J. W., R. Y. Zhang, G. H. Li, and W.-K. Tao, 2007b: Effects of aerosols and relative humidity on cumulus clouds. *J. Geophys. Res*., **112**, D14204, https://doi.org/10.1029/2006JD008136.

Fan, J. E., R. Y. Zhang, W.-K. Tao, and K. I. Mohr, 2008: Effects of aerosol optical properties on deep convective clouds and radiative forcing. *J. Geophys. Res*., **113**, D08209, https://doi.org/10.1029/2007JD009257.

Fan, J. W., L. R. Leung, Z. P. Li, H. Morrison, H. B. Chen, Y. Q. Zhou, Y. Qian, and Y. Wang, 2012: Aerosol impacts on clouds and precipitation in eastern China: Results from bin and bulk microphysics. *J. Geophys. Res*., **117**, D00K36, https://doi.org/10.1029/2011JD016537.

Fan, J. W., R. Y. Zhang, G. H. Li, W.-K. Tao, and X. W. Li, 2007a: Simulations of cumulus clouds using a spectral microphysics cloud-resolving model. *J. Geophys. Res*., **112**, D04201, https://doi.org/10.1029/2006JD007688.

Fan, J. W., Y. Wang, D. Rosenfeld, and X. H. Liu, 2016: Review of aerosol-cloud interactions: Mechanisms, significance, and challenges. *J. Atmos. Sci*., **73**(11), 4221–4252, https://doi.org/10.1175/JAS-D-16-0037.1.

Hansen, J., M. Sato, and R. Ruedy, 1997: Radiative forcing and climate response. *J. Geophys. Res*., **102**, 6831–6864, https://doi.org/10.1029/96JD03436.

IPCC, 2007: *Climate Change 2007: The Physical Science Basis. Contribution of Working group I to the Fourth Assessment Report of the Intergovernmental Panel on Climate Change*, S. Solomon et al., Eds., Cambridge University Press, Cambridge, United Kingdom, New York, NY, USA.

Jiang, J. H., and Coauthors, 2011: Influence of convection and aerosol pollution on ice cloud particle effective radius. *Atmos. Chem. Phys.* **11**, 457–463, https://doi.org/10.5194/acp-11-457-2011.

Johnson, B. T., K. P. Shine, and P. M. Forster, 2004: The semi-direct aerosol effect: Impact of absorbing aerosols on marine stratocumulus. *Quart. J. Roy. Meteor. Soc*., **130**, 1407–1422, https://doi.org/10.1256/qj.03.61.

Khain, A. P., 2009: Notes on state-of-the-art investigations of aerosol effects on precipitation: A critical review. *Environ. Res. Lett.*, **4**, 015004, https://doi.org/10.1088/1748-9326/4/1/015004.

Khalizov, A.F., H. Xue, L. Wang, J. Zheng, and R. Zhang, 2009: Enhanced light absorption and scattering by carbon soot aerosol internally mixed with sulfuric acid, *J. Phys. Chem. A*, **113**(6), 1066–1074, https://doi.org/10.1021/jp807531n.

Koren, I., G. Feingold, and L. A. Remer, 2010: The invigoration of deep convective clouds over the Atlantic: Aerosol effect, meteorology or retrieval artifact? *Atmos. Chem. Phys.*, **10**, 8855–8872, https://doi.org/10.5194/acp-10-8855-2010.

Koren, I., O. Altaratz, L. A. Remer, G. Feingold, J. V. Martins, and R. H. Heiblum, 2012: Aerosol-induced intensification of rain from the tropics to the mid-latitudes. *Nat. Geosci.*, **5**(2), 118–122, https://doi.org/10.1038/ngeo1364.

Lee, J., P. Yang, A. E. Dessler, B.-C. Gao, and S. Platnick, 2009: Distribution and radiative forcing of tropical thin cirrus clouds. *J. Atmos. Sci*., **66**, 3721–3731, https://doi.org/10.1175/2009JAS3183.1.

Lee, S. S., L. J. Donner, V. T. J. Phillips, and Y. Ming, 2008: The dependence of aerosol effects on clouds and precipitation on cloud-system organization, shear and stability. *J. Geophys. Res*., **113**, D16202, https://doi.org/10.1029/2007JD009224.

Levy, M. E., and Coauthors, 2013: Measurements of submicron aerosols in Houston, Texas during the 2009 SHARP field campaign. *J. Geophys. Res*., **118**, 10 518–10 534, https://doi.org/10.1002/jgrd.50785.

Li, G. H., Y. Wang, and R. Y. Zhang, 2008: Implementation of a two-moment bulk microphysics scheme to the WRF model to investigate aerosol-cloud interaction. *J. Geophys. Res*., **113**, D15211, https://doi.org/10.1029/2007JD009361.

Li, G. H., Y. Wang, K.-H. Lee, Y. W. Diao, and R. Y. Zhang, 2009: Impacts of aerosols on the development and precipitation of a mesoscale squall line. *J. Geophys. Res*., **114**, D17205, https://doi.org/10.1029/2008JD011581.

Li, Z. Q., F. Niu, J. W. Fan, Y. G. Liu, D. Rosenfeld, and Y. N. Ding, 2011: Long-term impacts of aerosols on the vertical development of clouds and precipitation. *Nature Geosci.*, **4**, 888–894, https://doi.org/10.1038/ngeo1313.

Lin, Y., Y. Wang, B. W. Pan, J. X. Hu, Y. G. Liu, and R. Y. Zhang, 2016: Distinct impacts of aerosols on an evolving continental cloud complex during the RACORO field campaign. *J. Atmos. Sci*., **73**(9), 3681–3700, https://doi.org/10.1175/jas-d-15-0361.1.

Liu, Y. G., and P. H. Daum, 2004: Parameterization of the autoconversion process. Part I: Analytical formulation of the Kessler-type parameterizations. *J. Atmos. Sci*., **61**(13), 1539–1548.

Mitchell, D. L., R. Zhang, and R. L. Pitter, 1990: The mass-dimensional relations for ice crystals and the influence of riming on the snowfall rate. *J. Appl. Meteor*., **29**, 153–163, https://doi.org/10.1175/1520-0450(1990)029<0153:MDRFIP>2.0.CO;2.

Nesbitt, S. W., R. Y. Zhang, and R. E. Orville, 2000: Seasonal and global NO_x production by lightning estimated from the optical transient detector (OTD). *Tellus B*, **52**, 1206–1215, https://doi.org/10.1034/j.1600-0889.2000.01121.x.

Orville, R. E., and Coauthors, 2001: Enhancement of cloud-to-ground lightning over Houston, Texas. *Geophys. Res. Lett*., **28**, 2597–2600, https://doi.org/10.1029/2001GL012990.

Peng, J. F., and Coauthors, 2016: Markedly enhanced absorption and direct radiative forcing of black carbon under polluted urban environments. *Proc. Natl. Acad. Sci. USA*, **113**, 4266–4271, https://doi.org/10.1073/pnas.1602310113.

Pincus, R., and M. B. Baker, 1994: Effect of precipitation on the albedo susceptibility of clouds in the marine boundary layer. *Nature*, **372**, 250–252, https://doi.org/10.1038/372250a0.

Rogers, R. R., and M. K. Yau, 1989: *A Short Course in Cloud Physics*. 3rd ed., Pergamon Press.

Rosenfeld, D., 1999: TRMM observed first direct evidence of smoke from forest fires inhibiting rainfall. *Geophys. Res. Lett*., **26**, 3105–3108, https://doi.org/10.1029/1999GL006066.

Rosenfeld, D., and Coauthors., 2014: Global observations of aerosol-cloud-precipitation-climate interactions. *Rev. Geophys*., **52**(4), 750–808, https://doi.org/10.1002/2013rg000441.

Rosenfeld, D., U. Lohmann, G. B. Raga, C. D. O'Dowd, M. Kulmala, S. Fuzzi, A. Reissell, and M. O. Andreae, 2008: Flood or drought: How do aerosols affect precipitation? *Science*, **321**, 1309–1313, https://doi.org/10.1126/science.1160606.

Sassen, K., and Coauthors, 1995: The 5-6 December 1991 FIRE IFO II jet stream cirrus case study: Possible influences of volcanic aerosols. *J. Atmos. Sci*., **52**, 97–123, https://doi.org/10.1175/1520-0469(1995)052<0097:TDFIIJ>2.0.CO;2.

Seifert, A., T. Heus, R. Pincus, and B. Stevens, 2015: Large-eddy simulation of the transient and near-equilibrium behavior of precipitating shallow convection. *Journal of Advances in Modeling Earth Systems*, **7**, 1918–1937, https://doi.org/10.1002/2015MS000489.

Stevens, B., and G. Feingold, 2009: Untangling aerosol effects on clouds and precipitation in a buffered system. *Nature*, **461**, 607–613, https://doi.org/10.1038/nature08281.

Ström, J., and S. Ohlsson, 1998: In situ measurements of enhanced crystal number densities in cirrus clouds caused by aircraft exhaust. *J. Geophys. Res*., **103**, 11 355–11 361, https://doi.org/10.1029/98JD00807.

Tao, W.-K., X. W. Li, A. Khain, T. Matsui, S. Lang, and J. Simpson, 2007: Role of atmospheric aerosol concentration on deep convective precipitation: Cloud-resolving model simulations. *J. Geophys. Res*., **112**, D24S18, https://doi.org/10.1029/2007JD008728.

Tao, W.-K., J.-P. Chen, Z. Q. Li, C. E. Wang, and C. D. Zhang, 2012: Impact of aerosols on convective clouds and precipitation. *Rev. Geophys*., **50**, RG2001, https://doi.org/10.1029/2011RG000369.

Twomey, S., 1977: The influence of pollution on the shortwave albedo of clouds. *J. Atmos. Sci*., **34**, 1149–1152, https://doi.org/10.1175/1520-0469(1977)034<1149:TIOPOT>2.0.CO;2.

Wang, Y., A. Khalizov, M. Levy, and R. Y. Zhang, 2013a: New directions: Light absorbing aerosols and their atmospheric impacts. *Atmos. Environ*., **81**, 713–715, https://doi.org/10.1016/j.atmosenv.2013.09.034.

Wang, Y., J. W. Fan, R. Y. Zhang, L. R. Leung, and C. Franklin, 2013b: Improving bulk microphysics parameterizations in simulations of aerosol indirect effects. *J. Geophys. Res*., **118**, 5361–5379, https://doi.org/10.1002/jgrd.50432.

Wang, Y., J. Jiang, H. Su, 2015: Atmospheric Responses to the Redistribution of Anthropogenic Aerosols, *J. Geophys. Res.*, **120**(18), 9625–9641, https://doi.org/10.1002/2015JD023665.

Wang, Y., K.-H. Lee, Y. Lin, M. Levy, R. Y. Zhang, 2014b: Distinct effects of anthropogenic aerosols on tropical cyclones. *Nat. Clim. Change*, **4**, 368–373, https://doi.org/10.1038/nclimate2144.

Wang, Y., Q. Wan, W. Meng, F. Liao, H. Tan, and R. Zhang, 2011: Long-term impacts of aerosols on precipitation and lightning over the pearl river delta megacity area in China. *Atmospheric Chemistry and Physics*, **11**, 12 421–12 436, https://doi.org/10.5194/acp-11-12421-2011.

Wang, Y., R. Y. Zhang, and R. Saravanan, 2014a: Asian pollution climatically modulates mid-latitude cyclones following hierarchical modelling and observational analysis. *Nat. Commun.*, **5**, 3098, https://doi.org/10.1038/ncomms4098.

Williams, E. R., R. Zhang, and J. Rydock, 1991: Mixed-phase microphysics and cloud electrification. *J. Atmos. Sci*., **48**, 2195–2203, https://doi.org/10.1175/1520-0469(1991)048<2195:MPMACE>2.0.CO;2.

Yuan, T. L., Z. Q. Li, R. Y. Zhang, and J. W. Fan, 2008: Increase of cloud droplet size with aerosol optical depth: An observation and modeling study. *J. Geophys. Res*., **113**, D04201, https://doi.org/10.1029/2007JD008632.

Zhang, M. H., S. Klein, D. Randall, R. Cederwall, and A. Del Genio, 2005: Introduction to special section on toward reducing cloud-climate feedback uncertainties in atmospheric general circulation models. *J. Geophys. Res*., **110**, D15S01, https://doi.org/10.1029/2005JD005923.

Zhang, R. Y., I. Suh, J. Zhao, D. Zhang, E. C. Fortner, X. X. Tie, L. T. Molina, and M. J. Molina, 2004: Atmospheric new particle formation enhanced by organic acids. *Science*, **304**, 1487–1490, https://doi.org/10.1126/science.1095139.

Zhang, R. Y., G. H. Li, J. W. Fan, D. L. Wu, and M. J. Molina, 2007: Intensification of pacific storm track linked to Asian pollution. *Proc. Nat. Acad. Sci.*, **104**, 5295–5299, https://doi.org/10.1073/pnas.0700618104.

Zhang, R. Y., and Coauthors, 2015: Formation of urban fine particulate matter. *Chem. Rev*., **115**(10), 3803–3855, https://doi.org/10.1021/acs.chemrev.5b00067.